Highly efficient broadband white-light emission in two-dimensional semi-conductive hybrid lead chlorides†

Yuyin Wang,[a] Chen Sun,[a] Bin Su,[b] Xianfeng Li,[c] Xiangxi Meng,[a] Huiru Lou,[a] Ziwen Cheng,[a] Ying Wang[a] and Guoming Lin *[d]

White-light emission (WLE) materials based on organic–inorganic hybrid lead halides have drawn considerable attention because of their applications in light-emission equipment. Despite considerable efforts, there is still a lack of two-dimensional (2D) lead-chlorine white-light emitting halides with high photoluminescence quantum efficiency (PLQE). Herein, we report the preparation of a new 2D layered hybrid halide, [DTHPE]Pb_4Cl_{10}, which exhibits bright wide-band WLE, a high PLQE of 8.86% and high anti-water stability. To the best of our knowledge, the PLQE of [DTHPE]Pb_4Cl_{10} exceeds that of most 2D lead chlorides. Furthermore, the emission intensity is unchanged even after continuous immersion in water for 7 days. Photoluminescence measurements indicate that the WLE originates from self-trapped excitons. [DTHPE]Pb_4Cl_{10} is a promising visible-blind UV hybrid halide owing to its excellent photoelectric response. [DTHPE]Pb_4Cl_{10} is an effective white-light emitting material for display applications. The coexistence of a high performance visible-blind UV response and high efficiency white-light emission provides attractive possibilities for potential applications in the multifunctional photoelectronic field.

Introduction

The development of highly efficient light emitting diodes (LEDs) has become increasingly important in recent years owing to their high energy efficiency and low negative impact on the environment. Of particular relevance are white-light-emitting diodes (WLEDs) that are rapidly replacing conventional incandescent and fluorescent lighting sources. Commercial WLEDs are usually manufactured by coating blue or UV chips with mixed-component phosphors. However, they exhibit several drawbacks, such as self-absorption, low efficiency and color instability. Single-component white-light-emitting materials can overcome these shortcomings, besides offering improved spectral stability, high color rendering index (CRI) and economic fabrication process. Owing to their broad application prospects in display devices and solid-state lighting, it is of great significance to develop high-quality single-component white-light-emitting materials.[1]

Hybrid lead halide semiconductors have attracted significant attention for application in optoelectronic devices, such as sensors, lasers, photovoltaic cells and LEDs.[2–6] Hybrid lead halide perovskites with diverse dimensional structures have been widely investigated due to their photoluminescence properties.[7–18] They exhibit ultra-high CRI values, large photoluminescence quantum efficiencies (PLQEs), and stable luminous colors.[19,20] Two-dimensional (2D) hybrid lead halide semiconducting compounds with wide-band white-light emission (WLE) typically exhibit excellent physical flexibility and good optical properties compared to other dimensional hybrid halide compounds.[21,22] Natural multiple quantum well structures in 2D layered hybrid halides restrict the number of carriers within the inorganic layer, resulting in good photoluminescence properties.[23,24]

Furthermore, various 2D hybrid luminous halides with unique optical and optoelectronic properties were synthesized by replacing the halide anions and the organic spacer cations to alter the layer thickness.[25–28] For instance, Karunadasa *et al.* employed a chain diamine for designing two novel 2D WLE materials, (EDBE)PbX_4 and (*N*-MEDA)PbX_4 (X = Cl or Br), that exhibit large CRIs.[29] Wang *et al.* identified a 2D hybrid white-light emitting halide, 2-methyl-1,5-diaminopentane, exhibiting

[a]*School of Chemistry, Chemical Engineering and Materials, Jining University, Qufu, Shandong, 273155, P. R. China*

[b]*School of Materials Science and Engineering in Tsinghua University, Tsinghua University, Beijing, 100000, P. R. China*

[c]*Institute of Nanotechnology (INT), Karlsruhe Institute of Technology (KIT), Hermann-von-Helmholtz Platz 1, 76344 Eggenstein-Leopoldshafen, Germany*

[d]*Department of Physics, National University of Singapore, Singapore 117551, Singapore. E-mail: lingmdbs@nus.edu.sg*

†Electronic supplementary information (ESI) available. CCDC 2167972. For ESI and crystallographic data in CIF or other electronic format see DOI: https://doi.org/10.1039/d2dt02108k

a PLQE of 3.37%.[30] Nonetheless, the rather low PLQE values of most 2D metal halide perovskites, such as (*N*-MEDA)$PbBr_4$ (0.5%), $(C_6H_5C_2H_4NH_3)_2PbCl_4$ (<1%), and $(C_4H_9NH_3)_2PbCl_4$ (1%), restrict their applications in photoluminescence.[29,31,32] Thus, it is imperative to develop new 2D hybrid semiconducting compounds with effective WLE for solid state lighting applications. In addition, self-trapped excitons, which are often found in materials with soft lattice and strong electron–phonon coupling, have attracted a lot of attention owing to their unique broadband emission and promising applications in persistent white light sources.

In this study, 1,2-di-3-(tetrahydropyrimidine) ethane (DTHPE) was synthesized *in situ* as a matching organic cation, and a new hybrid halide of [DTHPE]Pb_4Cl_{10} containing a 2D layer structure was prepared. The synergy of the soft crystal lattice and strong quantum confinement effect helps to achieve a PLQE of wideband WLE as high as 8.86%, exceeding that of most 2D lead chlorides previously reported. [DTHPE]Pb_4Cl_{10} exhibited bright wideband WLE with a CRI value of 84. Moreover, no significant degradation was observed after immersion in water for 7 days. Photoluminescence measurements indicate that WLE originates from self-trapped excitons. In addition, [DTHPE]Pb_4Cl_{10} is also a promising visible-blind UV hybrid halide owing to its excellent UV photoelectric response.

Experimental section

Synthesis of compound 1

$PbCl_2$ (0.4 mmol, 0.1112 g) and *N*,*N*′-bis(3-aminopropyl)-ethylenediamine (BAPrEDA, 0.7 mmol, 0.119 g) were mixed in a blended solution of dimethylformamide (DMF; 3 mL), H_2O (2 mL), and hydrochloric acid (HCl, 1 mL, 38%). The resulting solution was stirred at room temperature (RT) for 20 min, transferred to a 25 mL glass vial and sealed, and finally heated at 100 °C for 5 days. Colorless prismatic crystals were obtained after filtration and washed with ethanol. According to the structural analysis by single-crystal X-ray diffraction, these crystals correspond to [DTHPE]Pb_4Cl_{10} (compound **3**). The *in situ* reaction steps for the synthesis of DTHPE molecules are shown in Scheme S1 (ESI†). When HCl is used as a catalyst, the *N*-methylformamide/DMF molecule is readily hydrolyzed into formic acid at high temperatures. Subsequently, an intermediate product is formed *via* the nucleophilic substitution reaction between the two terminal amino groups of BAPrEDA and formic acid. Finally, the internal nucleophilic substitution reactions in compound **2** lead to the formation of the final DTHPE molecule (compound **3**). The terminal and internal nucleophilic substitution reactions on all the amino groups in BAPrEDA may simultaneously occur to form DTHPE molecules (Scheme S1†).

Methods

The XRD pattern of [DTHPE]Pb_4Cl_{10} was obtained using a Bruker D8 Advance X-ray powder diffractometer operated at 40 kV and 40 mA (Cu-Kα radiation, λ = 1.5418 Å). The solid-state ultraviolet-visible (UV-vis) absorption spectra of the powder specimens were recorded using a PE Lambda 900 UV-vis spectrophotometer in the wavelength range of 200 to 800 nm at RT. Thermogravimetric (TG) analyses were performed in the temperature range of RT–800 °C under a N_2 atmosphere using a Mettler TGA/SDTA 851 thermal analyzer.

Results and discussion

Structural description

Structural analysis indicates that [DTHPE]Pb_4Cl_{10} crystallizes in the orthorhombic structure in the centrosymmetric space group *Pbca* at a temperature of 296 K (Table S1†). Two crystallographically independent Pb^{2+} ions exist in the asymmetric structural unit of [DTHPE]Pb_4Cl_{10}. Both adopt unusual coordination modes with eight Cl atoms, including six Pb1–Cl bonds (2.752(3)–3.193(3) Å), two longer Pb1–Cl bonds (3.315(4) and 3.254(4) Å), six Pb2–Cl bonds (2.711(3)–3.190(4) Å), and two longer Pb2–Cl bonds (3.327(4) and 3.348(4) Å). [Pb(1)Cl6] and [Pb(2)Cl6] are interconnected by sharing faces to form a tetranuclear $[Pb_4Cl_{20}]$ cluster (Fig. 1a). In contrast to traditional 2D structures, the $[Pb_4Cl_{20}]$ cluster is further interconnected by sharing faces to form a 2D $[Pb_4Cl_{10}]^2$ layer in [DTHPE]Pb_4Cl_{10} (Fig. 1b). The 2D $[Pb_4Cl_{10}]^2$ layers are isolated and surrounded by organic $[DTHPE]^{2+}$ cations to form an ordinary 2D hybrid structure (Fig. 1c). Overall, the $[Pb_4Cl_{10}]^2$ layers and the $[DTHPE]^{2+}$ cations act as co-crystallized assembly blocks to form a typical organic–inorganic hybrid halide through C–H···Cl and N–H···Cl hydrogen bonds. The 2D $[Pb_4Cl_{10}]^2$ layers are isolated by the broadbandgap $[DTHPE]^{2+}$ cations, which avoids electronic interactions between the $[Pb_4Cl_{10}]^2$ layers. This enables the hybrid [DTHPE]Pb_4Cl_{10} to exhibit the intrinsic PL characteristics of the inorganic component. PXRD analysis was conducted using a Rigaku MiniFlex 600 diffractometer. The experimental data perfectly matched the calculated data (Fig. S1†), which confirmed the high phase purity of the [DTHPE]Pb_4Cl_{10} crystals.

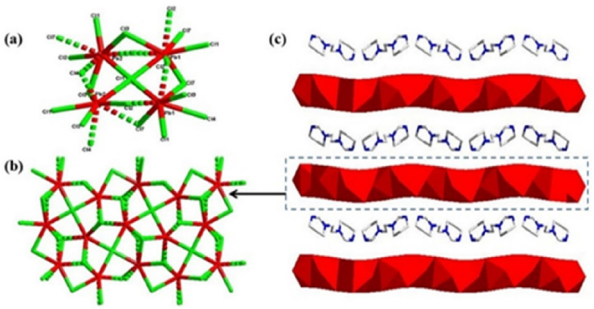

Fig. 1 Schematic representations of the (a) $[Pb_4Cl_{20}]^{12-}$ cluster, (b) 2D $[Pb_4Cl_{10}]^{2-}$ layer, and (c) packing structure of [DTHPE]Pb_4Cl_{10} along the *b*-axis. The red polyhedra represent $[PbCl_8]$ units.

Semiconducting performances

The potential of $[DTHPE]Pb_4Cl_{10}$ for photoelectronic applications was evaluated by measuring its optical and physical properties. The optical absorption spectrum shows that the location of absorption cut-off is 317 nm (Fig. S2a†). The optical bandgap was computed to be 3.92 eV according to the Tauc formula (Fig. S2b†).[33] Theoretical band structural calculation was conducted according to density functional theory (DFT) to obtain a more profound reference for the physical mechanism of $[DTHPE]Pb_4Cl_{10}$. Fig. 2a shows that both the conduction band minimum and valence band maximum are located at the *G* point, implying the direct bandgap semiconducting feature of $[DTHPE]Pb_4Cl_{10}$. The computed band structure exhibits a bandgap of 3.88 eV, which is slightly below the experimental value of 3.92 eV (Fig. 2a). Because of DFT restraints, these bandgap values are slightly different from the experimental values.[34] From the partial and total density of states (DOS) of $[DTHPE]Pb_4Cl_{10}$, the organic $[DTHPE]^{2+}$ cations were observed to contribute negligibly to the frontier optical and orbital properties. The highest occupied molecular orbital mainly comprises the overlap of the Pb-6s and Cl-3p states, and the lowest unoccupied molecular orbital results from the Pb-6p states (Fig. 2b).

Furthermore, to analyze the photoelectronic properties of $[DTHPE]Pb_4Cl_{10}$, a single-crystal lateral double-probe device was fabricated (Fig. S3†). Under 254 nm laser irradiation, the *I–V* relationship displayed a typical linear and symmetric trend (Fig. 2c), indicating excellent ohmic contact between $[DTHPE]Pb_4Cl_{10}$ and the Au electrodes. Meanwhile, the *I–V* curves were also measured under irradiation of 254 nm incident light. The *I–V* plots of the device exhibit typical symmetrical and linear features as the bias increases, which was attributed to the increase in the number of electron–hole pairs (Fig. 2c). The switching cycle of the single crystal photodetector was also investigated using a high-speed oscilloscope (Fig. 2d). After multiple switching cycles, the photocurrent still maintained a satisfactory fatigue-free state, which verifies the good stability of the single crystal photodetector. In addition, the rise time (t_r) and fall time (t_f) were measured only to be 200 μs and 400 μs, respectively (Fig. S4†), which is due to the low defect and trap densities in the high quality single crystal. Furthermore, the charge transport property was also investigated *via* space-charge-limited current (SCLC) measurements. At a voltage of 16 V, the logarithmic *I–V* curve shows the transformation of the ohmic region ($I \propto V$) to the trap-filled limit (TFL) region ($I \propto V^n$, $n > 3$) (Fig. S5†). In the ohmic region, the conductivity was 1.88×10^{-9} Ω cm^{-1} and the calculated trap density is 5.67×10^{10} cm^{-3} according to the following equation:

$$n_{trap} = \frac{2V_{TFL}\varepsilon\varepsilon_0}{eL^2} \quad (1)$$

where L is the distance of the conductive channel, ε is the relative dielectric constant, and e is the unit charge, while ε_0 represents the dielectric constant under vacuum. These properties are comparable to those of $MAPbCl_3$ single crystals,[35] demonstrating that $[DTHPE]Pb_4Cl_{10}$ is a promising candidate for high-performance visible-blind UV detectors.

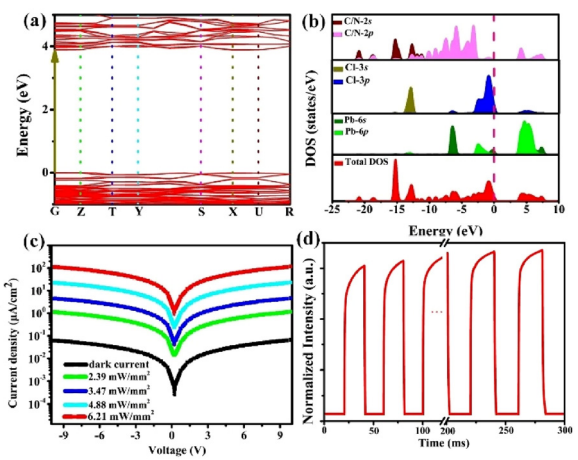

Fig. 2 (a) The calculated electronic band structure and (b) the partial and total DOSs of $[DTHPE]Pb_4Cl_{10}$; (c) the *J–V* curves obtained under dark conditions and at 365 nm UV light illumination with different power and (d) time-dependent switching cycles of the photocurrent response of a $[DTHPE]Pb_4Cl_{10}$ based photodetector.

Photoluminescence properties

When exposed to UV light with a wavelength of 366 nm, the $[DTHPE]Pb_4Cl_{10}$ crystals displayed bright white light visible to the naked eye (Fig. 3a). Under UV excitation at 366 nm, the crystals exhibit wide-band emission covering the entire visible spectrum with two maximum peaks at wavelengths of 443 and 550 nm (Fig. 3b). The Commission Internationale de l'Eclairage (CIE) 1931 chromaticity coordinates of $[DTHPE]Pb_4Cl_{10}$ (0.32, 0.35) are very close to those of standard pure WLE (0.33, 0.33) as shown in Fig. 3c. In addition, the CRI of $[DTHPE]Pb_4Cl_{10}$ (84) meets the requirements of most color-critical upmarket applications. Moreover, the color temperature of 6053 K corresponds to "cold" white light. Strikingly, the measured PLQE of $[DTHPE]Pb_4Cl_{10}$ was 8.86% (Fig. S6†), which is higher than that of most 2D lead chlorides (Table S5†), such as $(BZA)_2PbCl_4$ (BZA = $C_6H_5CH_2NH_3$, 3.57%) and $(H_2DABCO)Pb_2Cl_6$ (2.5%).[36,37] Furthermore, the $[DTHPE]Pb_4Cl_{10}$ crystals were continuously exposed to strong UV light (300 W cm^{-2}) for 100 h. The PL emission spectrum of the UV-irradiated sample still matches well with that of the as-synthesized sample. The PL decay and fitting curves obtained at 300 K and emission wavelengths of (Fig. 3e) 443 nm and (Fig. 3f) 550 nm were measured at different emission locations at the same excitation wavelength. At 443 nm, the PL decay curve of $[DTHPE]Pb_4Cl_{10}$ is fit using a biexponential function with average short (τ_1) and long (τ_2) lifetimes of 3.4495 and 12.5288 ns and occupancies of 50.88% (α_1) and 49.12% (α_2), respectively. A mean lifetime of 7.9092 ns (τ) is determined using the equation $\tau = \tau_1\alpha_1 + \tau_2\alpha_2$ (Fig. 3e). The τ_1 and τ_2 values at 550 nm are 1.7025 and 7.4226 ns, with α_1 and α_2 of 49.44%

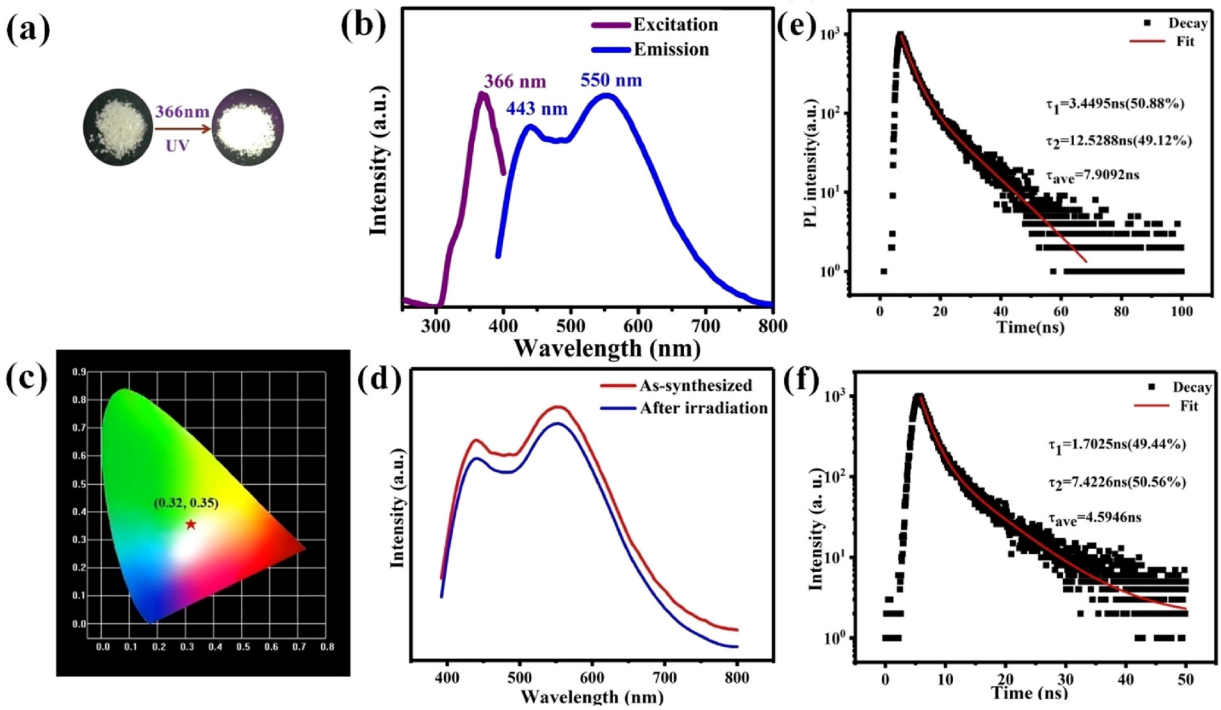

Fig. 3 (a) Images of crystals irradiated with ambient light and UV light (wavelength = 366 nm). (b) PL excitation and emission spectra of [DTHPE]Pb_4Cl_{10} upon UV light excitation at 366 nm. (c) CIE coordinates of [DTHPE]Pb_4Cl_{10}. (d) PL emission spectra of [DTHPE]Pb_4Cl_{10} before and after strong UV light irradiation for a long duration. PL decay and fit curves obtained at 300 K and at wavelengths of (e) 443 nm and (f) 550 nm.

and 50.56%, respectively. Consequently, the τ value at 550 nm is 4.5946 ns (Fig. 3f).

To confirm the photoluminescence characteristics obtained from the broadband excitation and emission spectra, we examined the wavelength-dependent spectra. A significant change was observed in the spectral profiles and peaks of wavelength-dependent excitation and emission spectra. This demonstrates that light emission in these cases is caused by relaxation from an identical excited state (Fig. S7†).

Meanwhile, green light emission with the maximum intensity at 520 nm was also observed in the PL excitation spectra of [DTHPE]Pb_4Cl_{10} at an excitation wavelength of 332 nm (Fig. 4a). The corresponding CIE chromaticity coordinates are (0.28, 0.35) (Fig. 4b). Moreover, the PL decay curve of [DTHPE]Pb_4Cl_{10} was fit with an average lifetime of 5.2164 ns (Fig. 4c). The PLQE of [DTHPE]Pb_4Cl_{10} is approximately 9.81% upon excitation with UV light at an excitation wavelength of 332 nm.

Photoluminescence mechanism

To confirm the intrinsic luminescence of [DTHPE]Pb_4Cl_{10} and eliminate the possibility of defect emission, the PL emission spectra of both bulk single crystals with diameters higher than 200 μm (Fig. S8a†) and microscale crystals with diameters lower than 10 μm (Fig. S8b†) were recorded. As shown in

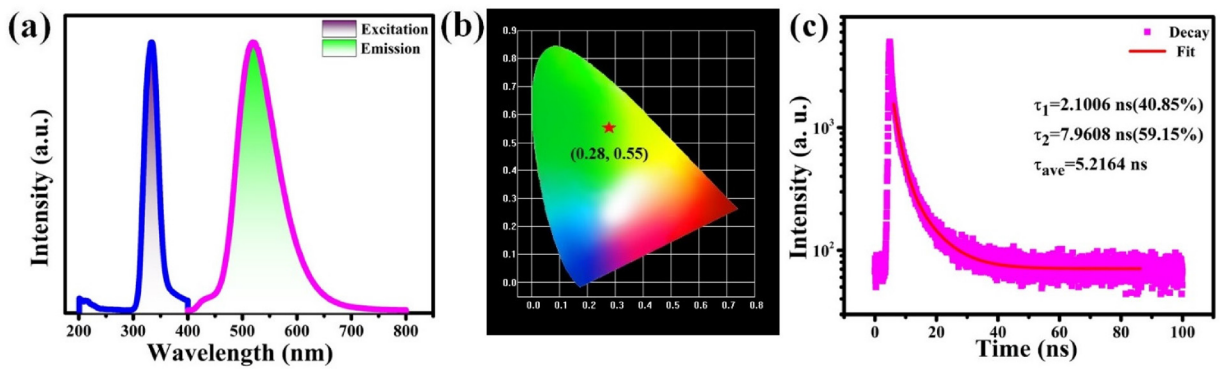

Fig. 4 (a) PL excitation and emission spectra of [DTHPE]Pb_4Cl_{10} upon UV light excitation at 332 nm. (b) CIE chromaticity coordinates of [DTHPE]Pb_4Cl_{10}. (c) PL decay curves of [DTHPE]Pb_4Cl_{10} at a temperature of 300 K.

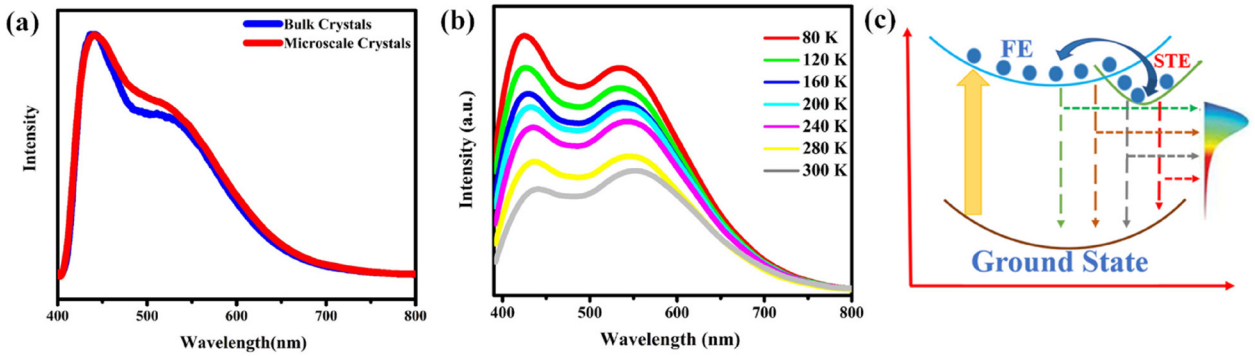

Fig. 5 (a) PL spectra of bulk crystals and microscale crystals of [DTHPE]Pb_4Cl_{10}. (b) Temperature-dependent emission spectra obtained upon UV light excitation at 366 nm. (c) Schematic of the proposed PL mechanism.

Fig. 5a, the emission spectrum of microscale crystals is similar to that of the bulk crystal and the intensity is only slightly lower indicating the absence of surface defect emission. To further examine the PL emission mechanism and validate the mechanism of wide-band WLE in [DTHPE]Pb_4Cl_{10}, temperature-dependent emission spectra were recorded in the temperature range of 80 to 300 K (Fig. 5b). No emission splitting phenomenon is observed with a decrease of test temperature indicating a single radiative mechanism. The wide-band emission intensity increases rapidly with a decrease of temperature. In general, photogenerated free carriers initially form free excitons (FEs) and then relax into distorted self-trapped excitons (STEs) due to electron–phonon coupling.[38–40] However, STEs can also be thermally detrapped to form FEs. At low temperatures, the thermal energy is inadequate to release the carriers from the STE to the FE state, thereby increasing the wide-band emission intensity. The coexistence of FEs and STEs can be described using a configuration coordinate diagram (Fig. 5c). The behaviors of the narrow-band and the wide-band emissions reveal the significance of STEs (within the distorted lattice) in [DTHPE]Pb_4Cl_{10} in the generation of WLE. The photogenerated carriers could be self-trapped in the excited state, causing wide-band emission because of the robust electron–phonon coupling in the distorted lattice.[41–43] Moreover, as shown in Fig. 5b, the wide-band emission at ~410 nm largely increased as the temperature decreased which means that the carrier transport from the FE to the STE state is also blocked. Energy release between the STE and the FE state is blocked owing to the low temperature, so that the emission at both ~410 nm and ~530 nm could be increased, which is consistent with the mechanism.

Stability

For practical applications of WLE devices, durability is closely related to the thermal stability and anti-water stability of metal halide hybrid crystals. Fig. 6a shows the PXRD patterns of [DTHPE]Pb_4Cl_{10} after submersion in water for different days. It is evident that the PXRD patterns are unaltered after submersion. Moreover, the PL spectra of [DTHPE]Pb_4Cl_{10} (Fig. 6b) do not show significant variations after submersion in water for 1, 3, 5, and 7 days. Moreover, there is no significant drop in the intensity of emission compared to the initial value. These indicate the excellent humidity stability of [DTHPE]Pb_4Cl_{10} crystals. TG analysis reveals that [DTHPE]Pb_4Cl_{10} is stable below 333 °C (Fig. S9†), and the PXRD patterns do not change at different temperatures, indicating sufficient thermal stability (Fig. 6c). These results suggest that [DTHPE]Pb_4Cl_{10} is a promising candidate for solid state lighting applications. To

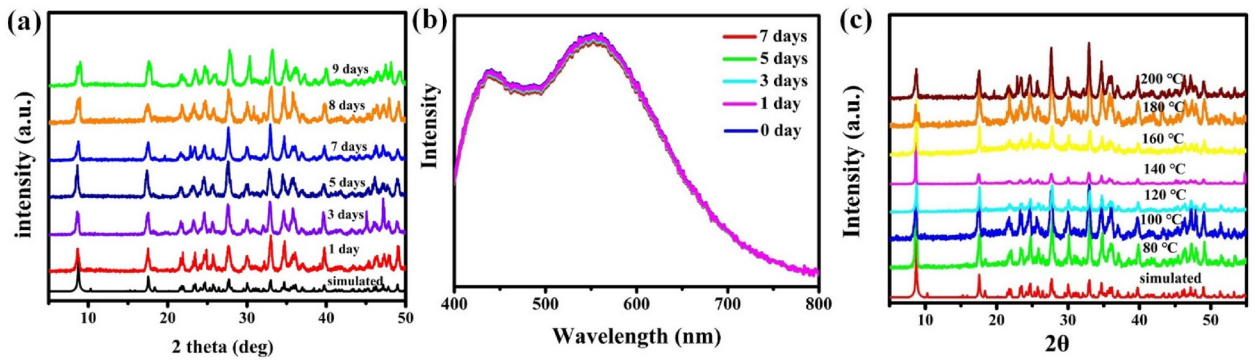

Fig. 6 (a) Comparisons of the (a) PXRD patterns and (b) PL spectra of the crystals of [DTHPE]Pb_4Cl_{10} before and after submersion in water for a period of 1, 3, 5, 7, 8, and 9 days. (c) PXRD patterns of [DTHPE]Pb_4Cl_{10} at different temperatures.

further validate WLE from [DTHPE]Pb_4Cl_{10}, a 365 nm UV-LED lamp was introduced. A thin layer of [DTHPE]Pb_4Cl_{10} prepared using the supersaturated solution was coated onto the LED lamp. When illuminated, bright white light from the compound is observed (Fig. S10†).

Conclusions

In summary, a novel 2D organic–inorganic hybrid perovskite semiconductor, [DTHPE]Pb_4Cl_{10}, with highly efficient white-light-emitting properties was developed, which simultaneously exhibits excellent semiconductor properties, a high CRI of 84, and a high PLQE of 8.86%. The PLQE of [DTHPE]Pb_4Cl_{10} is higher than those of most 2D white-light-emitting hybrid lead chlorides. In addition, [DTHPE]Pb_4Cl_{10} exhibited a high UV photoelectric response and low trap density. No degradation was observed after immersion in water for 7 days, indicating the excellent anti-water stability of [DTHPE]Pb_4Cl_{10}. The findings of this study are expected to pave the way for further design and development of materials that efficiently emit white light for solid-state lighting applications.

Conflicts of interest

The authors declare no conflicts of interest.

Acknowledgements

The authors are grateful for the financial support from the National Natural Science Foundation of China (no. 22101282), the Shandong Provincial Natural Science Foundation Youth Fund (ZR2021QB204), and the Jining University 2019, 2020 "100 Outstanding Talents" support program cultivation project (2020ZYRC02).

References

1 Y. Wei, Z. Cheng and J. Lin, *Chem. Soc. Rev.*, 2019, **48**, 310–350.

2 (*a*) W. Xu, Q. Hu, S. Bai, C. Bao, Y. Miao, Z. Yuan, T. Borzda, A. J. Barker, E. Tyukalova, Z. Hu, M. Kawecki, H. Wang, Z. Yan, X. Liu, X. Shi, K. Uvdal, M. Fahlman, W. Zhang, M. Duchamp, J.-M. Liu, A. Petrozza, J. Wang, L.-M. Liu, W. Huang and F. Gao, *Nat. Photonics*, 2019, **13**, 418–424; (*b*) M. Z. Li and Z. G. Xia, *Chem. Soc. Rev.*, 2021, **50**, 2626–2662; (*c*) X. L. Song, G. F. Wei, J. Sun, C. D. Peng, J. L. Yin, X. Zhang, Y. L. Jiang and H. H. Fei, *Nat. Catal.*, 2020, **3**, 1027–1033; (*d*) J. L. Yin, H. M. Yang and H. H. Fei, *Chem. Mater.*, 2019, **31**, 3909–3916.

3 (*a*) G. Xing, N. Mathews, S. S. Lim, N. Yantara, X. Liu, D. Sabba, M. Gratzel, S. Mhaisalkar and T. C. Sum, *Nat. Mater.*, 2014, **13**, 476–480; (*b*) G. J. Zhou, Z. Y. Liu, J. L. Huang, M. S. Molokeev, Z. W. Xiao, C. G. Ma and Z. G. Xia, *J. Phys. Chem. Lett.*, 2020, **11**, 5956–5962.

4 (*a*) A. A. M. Brown, T. J. N. Hooper, S. A. Veldhuis, X. Y. Chin, A. Bruno, P. Vashishtha, J. N. Tey, L. Jiang, B. Damodaran, S. H. Pu, S. G. Mhaisalkar and N. Mathews, *Nanoscale*, 2019, **11**, 12370–12380; (*b*) K. Li, Z.-G. Li, J. Xu, Y. Qin, W. Li, A. Stroppa, K. T. Butler, C. J. Howard, M. T. Dove, A. K. Cheetham and X.-H. Bu, *J. Am. Chem. Soc.*, 2022, **144**, 816–823; (*c*) F.-F. Gao, X. Li, Y. Qin, Z.-G. Li, T.-M. Guo, Z.-Z. Zhang, G.-D. Su, C. Jiang, M. Azeem, W. Li, X. Wu and X.-H. Bu, *Adv. Opt. Mater.*, 2021, **9**, 2100003.

5 P. Cai, X. Wang, H. J. Seo and X. Yan, *Appl. Phys. Lett.*, 2018, **112**, 153901.

6 S. A. Veldhuis, P. P. Boix, N. Yantara, M. Li, T. C. Sum, N. Mathews and S. G. Mhaisalkar, *Adv. Mater.*, 2016, **28**, 6804–6834.

7 L. Li, X. Liu, Y. Li, Z. Xu, Z. Wu, S. Han, K. Tao, M. Hong, J. Luo and Z. Sun, *J. Am. Chem. Soc.*, 2019, **141**, 2623–2629.

8 M. Bidikoudi, E. Fresta and R. D. Costa, *Chem. Commun.*, 2018, **54**, 8150–8169.

9 I. Neogi, A. Bruno, D. Bahulayan, T. W. Goh, B. Ghosh, R. Ganguly, D. Cortecchia, T. C. Sum, C. Soci, N. Mathews and S. G. Mhaisalkar, *ChemSusChem*, 2017, **10**, 3765–3772.

10 L. Mao, P. Guo, M. Kepenekian, I. Hadar, C. Katan, J. Even, R. D. Schaller, C. C. Stoumpos and M. G. Kanatzidis, *J. Am. Chem. Soc.*, 2018, **140**, 13078–13088.

11 D. Li, W. Wu, S. Wang, X. Zhang, L. Li, Y. Yao, Y. Peng and J. Luo, *J. Mater. Chem. C*, 2020, **8**, 6710–6714.

12 C.-Y. Yue, H.-X. Sun, Q.-X. Liu, X.-M. Wang, Z.-S. Yuan, J. Wang, J.-H. Wu, B. Hu and X.-W. Lei, *Inorg. Chem. Front.*, 2019, **6**, 2709–2717.

13 S. Elleuch, A. Lusson, S. Pillet, K. Boukheddaden and Y. Abid, *ACS Photonics*, 2020, **7**, 1178–1187.

14 M. Konstantakou and T. Stergiopoulos, *J. Mater. Chem. A*, 2017, **5**, 11518–11549.

15 Z. Yuan, C. Zhou, Y. Tian, Y. Shu, J. Messier, J. C. Wang, L. J. van de Burgt, K. Kountouriotis, Y. Xin, E. Holt, K. Schanze, R. Clark, T. Siegrist and B. Ma, *Nat. Commun.*, 2017, **8**, 14051.

16 P. Shen, T. Vogt and Y. Lee, *J. Phys. Chem. Lett.*, 2020, **11**, 4131–4137.

17 J. Luo, X. Wang, S. Li, J. Liu, Y. Guo, G. Niu, L. Yao, Y. Fu, L. Gao, Q. Dong, C. Zhao, M. Leng, F. Ma, W. Liang, L. Wang, S. Jin, J. Han, L. Zhang, J. Etheridge, J. Wang, Y. Yan, E. H. Sargent and J. Tang, *Nature*, 2018, **563**, 541–545.

18 R. Gautier, M. Paris and F. Massuyeau, *J. Am. Chem. Soc.*, 2019, **141**, 12619–12623.

19 Y. Peng, Y. Yao, L. Li, Z. Wu, S. Wang and J. Luo, *J. Mater. Chem. C*, 2018, **6**, 6033–6037.

20 S. Yang, Z. Lin, J. Wang, Y. Chen, Z. Liu, E. Yang, J. Zhang and Q. Ling, *ACS Appl. Mater. Interfaces*, 2018, **10**, 15980–15987.

21 E. Shi, Y. Gao, B. P. Finkenauer, Akriti, A. H. Coffey and L. Dou, *Chem. Soc. Rev.*, 2018, **47**, 6046–6072.

22 Z. Wu, C. Ji, Z. Sun, S. Wang, S. Zhao, W. Zhang, L. Li and J. Luo, *J. Mater. Chem. C*, 2018, **6**, 1171–1175.

23 L. Li, X. Shang, S. Wang, N. Dong, C. Ji, X. Chen, S. Zhao, J. Wang, Z. Sun, M. Hong and J. Luo, *J. Am. Chem. Soc.*, 2018, **140**, 6806–6809.

24 L. M. Castro-Castro and A. M. Guloy, *Angew. Chem., Int. Ed.*, 2003, **42**, 2771–2774.

25 G. Zhou, M. Li, J. Zhao, M. S. Molokeev and Z. Xia, *Adv. Opt. Mater.*, 2019, **7**, 1901335.

26 L. Mao, Y. Wu, C. C. Stoumpos, M. R. Wasielewski and M. G. Kanatzidis, *J. Am. Chem. Soc.*, 2017, **139**, 5210–5215.

27 L. Mao, Y. Wu, C. C. Stoumpos, B. Traore, C. Katan, J. Even, M. R. Wasielewski and M. G. Kanatzidis, *J. Am. Chem. Soc.*, 2017, **139**, 11956–11963.

28 A. Yangui, D. Garrot, J. S. Lauret, A. Lusson, G. Bouchez, E. Deleporte, S. Pillet, E. E. Bendeif, M. Castro, S. Triki, Y. Abid and K. Boukheddaden, *J. Phys. Chem. C*, 2015, **119**, 23638–23647.

29 E. R. Dohner, A. Jaffe, L. R. Bradshaw and H. I. Karunadasa, *J. Am. Chem. Soc.*, 2014, **136**, 13154–13157.

30 S. Wang, Y. Yao, J. Kong, S. Zhao, Z. Sun, Z. Wu, L. Li and J. Luo, *Chem. Commun.*, 2018, **54**, 4053–4056.

31 C. Ji, S. Wang, L. Li, Z. Sun, M. Hong and J. Luo, *Adv. Funct. Mater.*, 2018, **29**, 1805038.

32 K. Thirumal, W. K. Chong, W. Xie, R. Ganguly, S. K. Muduli, M. Sherburne, M. Asta, S. Mhaisalkar, T. C. Sum, H. S. Soo and N. Mathews, *Chem. Mater.*, 2017, **29**, 3947–3953.

33 J. Tauc, R. Grigorovici and A. Vancu, *Phys. Status Solidi B*, 1996, **15**, 627–637.

34 (*a*) R. W. Godby, M. Schluther and L. J. Sham, *Phys. Rev. B: Condens. Matter Mater. Phys.*, 1987, **36**, 6497–6450; (*b*) R. Terki, G. Bertrand and H. Aourag, *Microelectron. Eng.*, 2005, **81**, 514–523.

35 (*a*) G. Maculan, A. D. Sheikh, A. L. Abdelhady, M. I. Saidaminov, M. A. Haque, B. Murali, E. Alarousu, O. F. Mohammed, T. Wu and O. M. Bakr, *J. Phys. Chem. Lett.*, 2015, **6**, 3781–3786; (*b*) A. Poglitsch and D. Weber, *J. Chem. Phys.*, 1987, **87**, 6373–6378.

36 M. H. Jung, *Inorg. Chem.*, 2019, **58**, 6748–6757.

37 G. E. Wang, G. Xu, M. S. Wang, L. Z. Cai, W. H. Li and G. C. Guo, *Chem. Sci.*, 2015, **6**, 7222–7226.

38 J.-Q. Zhao, C. Sun, M. Yue, Y. Meng, X.-M. Zhao, L.-R. Zeng, G. Chen, C.-Y. Yue and X.-W. Lei, *Chem. Commun.*, 2021, **57**, 1218–1221.

39 A. Yangui, D. Garrot, J. S. Lauret, A. Lusson, G. Bouchez, E. Deleporte, S. Pillet, E. E. Bendeif, M. Castro, S. Triki, Y. Abid and K. Boukheddaden, *J. Phys. Chem. C*, 2015, **119**, 23638–23647.

40 Z. Yuan, C. K. Zhou, Y. Tian, Y. Shu, J. Messier, J. C. Wang, L. J. van de Burgt, K. Kountouriotis, Y. Xin, E. Holt, K. Schanze, R. Clark, T. Siegrist and B. Ma, *Nat. Commun.*, 2017, **8**, 14051.

41 B. K. Ridley, *J. Phys. C: Solid State Phys.*, 1982, **15**, 5899.

42 V. V. Kabanov and O. Y. Mashtakov, *Phys. Rev. B: Condens. Matter Mater. Phys.*, 1993, **47**, 6060–6064.

43 Y. Toyozawa, *Prog. Theor. Phys.*, 1961, **26**, 29–44.